Hybrid Strategy to Simulate 3-D Nonlinear Radio-Frequency Ultrasound Using a Variant Spatial PSF

François Varray, Olivier Bernard, Sonia Assou, Christian Cachard, and Didier Vray

***Abstract*— There are several simulators for medical ultrasound (US) applications that can fully compute the nonlinear propagation on the transmitted pulse and the corresponding radio-frequency (RF) images. Creanuis is one recent model used to generate nonlinear RF images; however, the time requirements are long compared with linear models using a convolution strategy. In this paper, we describe an approach using convolution coupled with nonlinear information to create a pseudoacoustic tool that is able to quickly generate realistic US images. Several point-spread functions (PSFs) are computed with Creanuis. These PSFs are extracted at different depths in order to take into account variation in the resolution and apparition of harmonics during propagation. One convolution is then conducted for each PSF to generate a set of nonlinear raw RF images. The final image is obtained by merging these raw images using a PSF-weighting function. This hybrid Creanuis strategy was extended to 2-D, 2-D + t, 3-D, and 3-D + t images for both linear and phased-array geometries. We validated h-Creanuis using the mean deviation between the proposed images and those created using Creanuis and examined their statistical distributions. The mean deviations of Creanuis and h-Creanuis are below 2.5% for fundamental and second-harmonic images. The 3-D + t images obtained demonstrate the correct motion characteristics for speckle in sequences of both fundamental and second-harmonic images.**

***Index Terms*— Creanuis, image simulation, nonlinear propagation.**

I. Introduction

VARIOUS simulation tools are available for the generation of ultrasound (US) radio-frequency (RF) images. The use of numerical models allows US images with known characteristics to be generated. These are mainly used to test, validate, and improve methodological developments. The proposed simulation tools are mainly based on the following:

1) full acoustic models utilized in the image simulation software Field II [1] and Creanuis [2];
2) linear convolution models, such as Creasimus [3] and Cole [4], [5];
3) full-wave models in which backscattered signals are created by fully integrating the wave propagation [6], [7].

The advantage of a full acoustic model is that the effects of various physical parameters of the probe can be considered, such as the number of active elements, spatial impulse response, focalization, and apodization, in both transmission and reception, as in the case of Field II [1]. In such a model, the transducer properties are taken into account during both transmission and reception. The transmitted wave is then computed using a forward model and echoes are generated using point scatterers. In comparison with Field II, Creanuis takes into consideration the nonlinear propagation of the US waves within the media [8] and then generates the corresponding harmonic images. This feature is essential for developing and testing nonlinear imaging techniques such as pulse inversion (PI) [9], amplitude modulation [10], and their derivatives.

The principle of linear methods is based on the convolution of a given point-spread function (PSF), either simulated or measured, with a set of scatterers. With these techniques, a unique PSF is used, which produces a constant speckle resolution as a function of depth. By employing such a mathematical background, the computation time is strongly reduced in comparison with all other methods, and US sequences can be easily simulated. Such methods are of particular interest for training purposes [11], [12]. In the work described here, ray tracing was used on a computed tomography image in order to compute a map of the acoustic reflections and shadowing effects. The US images were then obtained by convolving this map with the desired PSF. In Creasimus [3], the convolution is performed between a Gaussian 3-D PSF and a scatterer map, a sequence similar to the one in Field II. The elevation direction of the scatterers is considered by projection in the imaging plane. In the software Cole, the lateral evolution of the resolution as a function of depth is included, thanks to complementary computing [4]. However, with these linear models, the nonlinear distortion of the pressure wave is not computed and harmonic imaging is not currently available.

Several strategies have been proposed that use the full-wave equation to solve the linear and nonlinear wave propagation in media in which the speed of sound, density, and coefficient of nonlinearity are inhomogeneous [6], [7]. In these situations, the scatterers are not defined, because the image is directly related to the impedance change inside the simulated medium.

AQ:1 Manuscript received January 25, 2016; accepted June 5, 2016. Date of publication June 10, 2016. This work was supported by the French National Research Agency, Université de Lyon, within the Framework of the LabEx CeLyA and LabEx PRIMES through the Program Investissements
AQ:2 d'Avenir under Grant ANR-10-LABX-0060, Grant ANR-11-LABX-006, and Grant ANR-11-IDEX-0007. *(Corresponding author: François Varray.)*

AQ:3 The authors are with the Centre National de la Recherche Scientifique, Centre de Recherche en Acquisition et Traitement de l'Image pour la Santé, Inserm, Institut National des Sciences Appliquées de Lyon, Université de Lyon, Université Lyon 1, Lyon F-69621, France (e-mail: francois.varray@creatis.insa-lyon.fr; olivier.bernard@creatis.insa-lyon.fr; sonia_a@live.fr; christian.cachard@creatis.insa-lyon.fr; didier.vray@creatis.insa-lyon.fr).

Digital Object Identifier 10.1109/TUFFC.2016.2579666

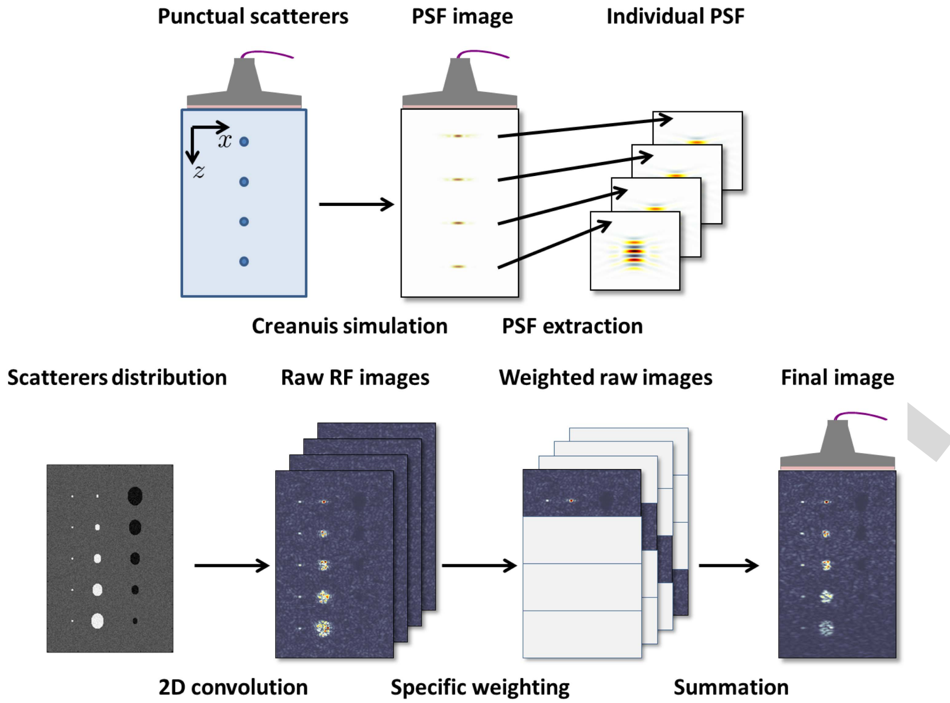

Fig. 1. h-Creanuis simulation pipeline. The PSFs are extracted at various depths from the reference point scatterers and one Creanuis simulation. Raw US images are then generated using 2-D convolution. Specific PSF-weighting is used to create the final h-Creanuis image.

From this perspective, the obtained images are more realistic. The simulation of the whole image implies a new full-wave simulation for each raw RF line. However, full-wave methods usually exhibit a long computation time and a large amount of memory is required. Moreover, to accurately simulate the transducer geometry and its spatial impulse response, a fine grid discretization is necessary and will continue to increase both computation time and memory requirement. Fast simulation tools capable of modeling nonlinear and other complex phenomena in US remain of interest.

The objective of this paper is to propose a new strategy to simulate RF images with depth-varying PSF and harmonic components. To this end, we combined the acoustic model of Creanuis with a convolution-based method. Indeed, using Creanuis will directly integrate the harmonic information in the RF image. Usually, only one PSF is used to simulate the full US image. However, this PSF is not constant for the whole axial range and has to theoretically be updated in the function of the depth. In this paper, we propose to compute several PSFs at different depths in order to take into account the PSF-depth evolution. We recently applied this kind of approach, previously used for linear arrays, to generate 2-D harmonic images with a spatially varying PSF [13]. In this paper, we extend this hybrid Creanuis (h-Creanuis) model to simulate 2-D + t, 3-D, and 3-D + t image sequences. The next section presents the methodology of h-Creanuis, which is then illustrated in various examples in Section III. A discussion presented in Section V concludes this paper.

II. Methodology of h-Creanuis

Various steps are necessary to simulate an h-Creanuis nonlinear US image: 1) different PSFs are computed for different depths; 2) the corresponding raw images are computed; and 3) the individual convolved images are combined to obtain the h-Creanuis image. The complete scheme of the h-Creanuis strategy is shown in Fig. 1.

A. Linear Array Geometry

1) Extraction of the PSF: In the general scheme of Creasimus, the PSF is defined as a 3-D Gaussian kernel [3]. The parameters of this kernel are generated in an arbitrary manner and are not related to the probe or beamforming strategy. Creanuis software is used to simulate realistic PSFs with varying resolution and signal-to-noise (SNR) as a function of depth. A medium with N point scatterers is thereby generated [2]. The resulting PSFs are now related to the probe size, image beamforming, and the characteristic of the medium and vary in both axial and lateral directions. Moreover, the nonlinear distortion of the propagating pressure wave is taken into account and both fundamental and second-harmonic components are contained in the simulated temporal PSF. This simulation is conducted using a physical probe description (number of active elements, sampling frequency, and pitch) and a beamforming strategy. Based on GPU programming of the nonlinear field computation, the total computation time is reduced [14]. To compute the PSFs, the simulation is conducted only with N scatterers placed at the (x_i, y_i, z_i) location

$$\begin{cases} x_i = 0 \\ y_i = 0 \\ z_i = \dfrac{2i-1}{2N}(z_{\max} - z_{\min}) + z_{\min} \end{cases} \tag{1}$$

where i is the ith scatterer and $z_{\min}$ and $z_{\max}$ are the minimal and maximal depths of the simulated image, respectively.

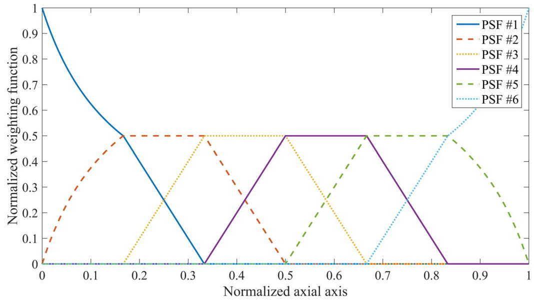

Fig. 2. Amplitude as a function of the axial axis for the six PSFs used.

The N nonlinear PSFs are extracted after the Creanuis simulation of the RF image.

2) Simulating Raw Images: The first step is the generation of the desired distribution of medium scatterers (3-D positions and amplitudes). The Creasimus methodology background is then used [3] to simulate each nonlinear raw RF image, named I_i, with one of the extracted PSFs at depth z_i. The convolution is conducted in 2-D and the elevation direction of the scatterer has to be taken into account; this was proposed and validated in this previous methodology. With N different PSFs, corresponding to the N different depths, N nonlinear raw RF images are obtained. Each image has a constant resolution and SNR for the various depths, which is related to the ith PSF used. However, because the amplitude of the pressure wave varies for each PSF, the resolution and SNR are different for each nonlinear raw RF image. The value of N is validated in experimental work.

3) Creating Final Images: The N nonlinear raw RF images are now combined. A weighting function W_i is defined for each raw RF image. The W_i weighting function should be maximal at the depth corresponding to the ith PSF and null elsewhere. Six weighting functions are illustrated in Fig. 2. The formula is based on constant and linear amplitudes depending on the z-axis. They are then normalized together in order to obtain

$$\forall z \in \mathbb{R}, \quad \sum_{i=1}^{N} W_i(z) = 1. \tag{2}$$

The final RF image is then obtained by merging the different raw images, where each of them has a modified amplitude

$$\mathrm{Im} = \sum_{i=1}^{N} I_i \times W_i. \tag{3}$$

The final image Im contains the nonlinear components of each raw image and a depth evolution of the resolution and SNR. To obtain and display only the fundamental or second-harmonic image, the RF image is filtered with a fourth-order Butterworth bandpass filter centered on the fundamental or second-harmonic frequency.

B. Phased-Array and 3-D Geometry

Simulation of sectorial scans using a linear array requires the use of the same strategy. However, the position of each scatterer (x, z) needs to be recalculated before generating the nonlinear raw RF images. The details of the calculation can

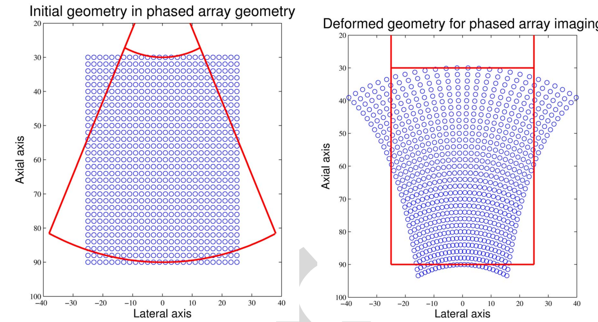

(a) (b)

Fig. 3. Illustration of the phased-array geometry (a) before and (b) after updating the scatterers for the simulation.

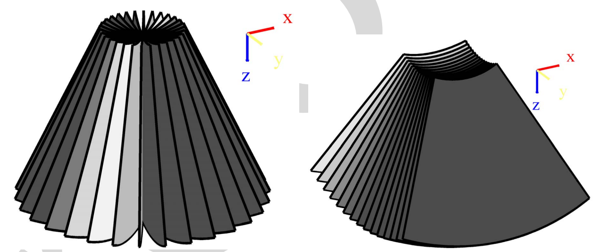

(a) (b)

Fig. 4. Scanning strategy for 3-D images. (a) Pyramidal scan. (b) Full 3-D phased-array scan.

be found in the Appendix. A regular grid of scatterers before and after such a conversion is illustrated in Fig. 3. After this conversion, h-Creanuis is used to simulate the image and the resulting image is then remapped onto the initial geometry, as displayed inside the red lines in Fig. 3(a).

To simulate 3-D h-Creanuis images, a strategy was designed to simulate the whole 3-D nonlinear image in a pyramidal or full phased-array scan, similar to the one used for 2-D phased-array image simulation. Following simulation, the 3-D image stack is remapped onto a Cartesian grid to facilitate visualization. The two kinds of scanning strategies are illustrated in Fig. 4. The mathematical details can be found in the Appendix.

III. Results

A. 2-D h-Creanuis Evaluation

1) General Overview: To test the h-Creanuis method, an image of a numerical cyst phantom [15] was simulated using six different PSFs ($N = 6$). The number of PSFs is discussed later in this section. This phantom is well adapted because it is composed of hyperechoic and hypoechoic regions as well as point scatterers. It is then easier to evaluate the resolution and SNR. The phantom is composed of 100 000 3-D scatterers. The nonlinear images were simulated using both Creanuis and h-Creanuis. The parameters used in the Creanuis simulation are presented in Table I. Three raw simulated fundamental and second-harmonic log-compressed images corresponding to PSFs #1, #2, and #5 are shown in Fig. 5. They have been normalized with the same value and have a 40-dB

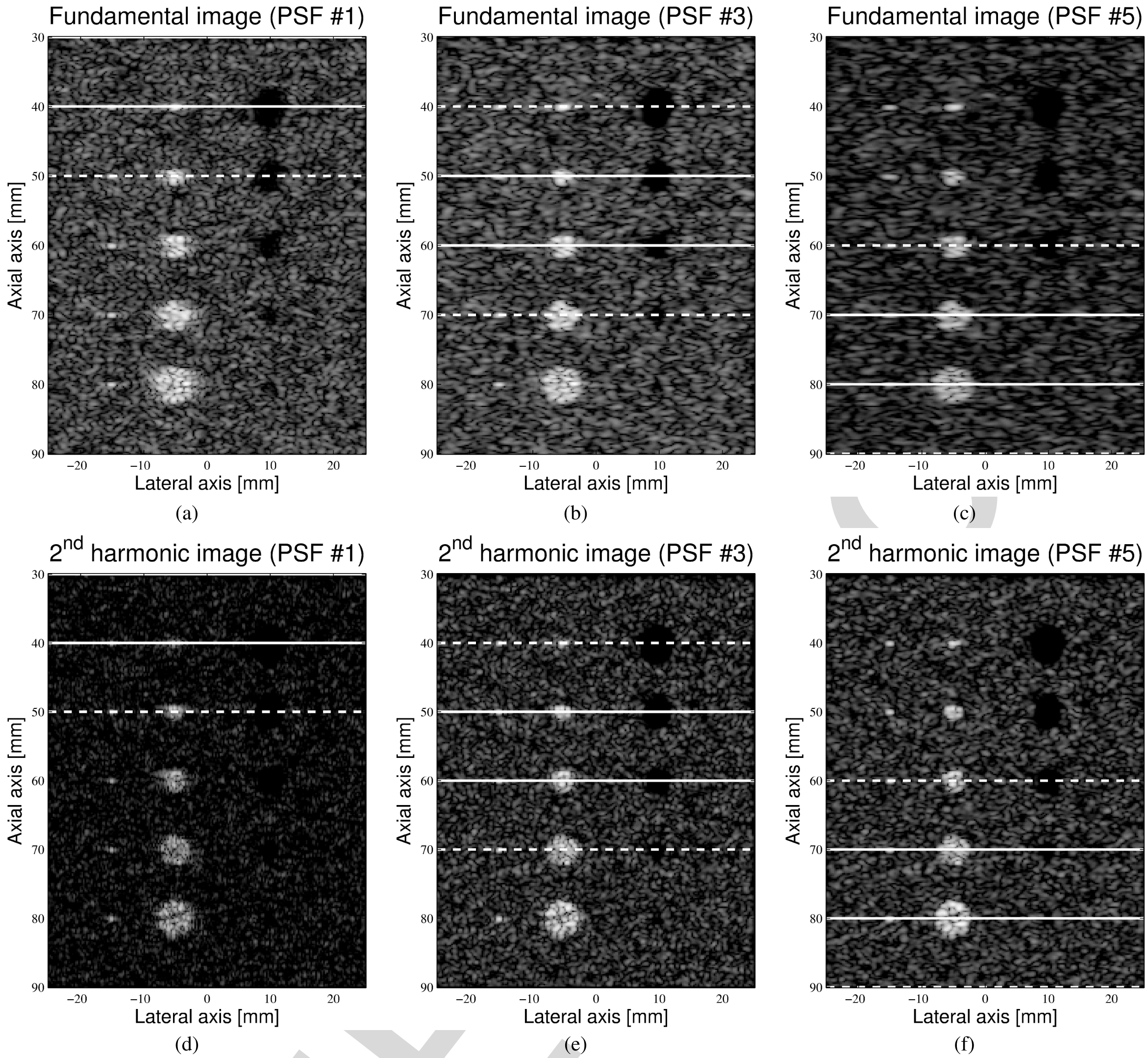

Fig. 5. Simulated raw images for PSFs #1, #3, and #5. The first line corresponds to fundamental images and the second line to second-harmonic images. On each image, the region between the two lines corresponds to a section where the weighting amplitude function is maximal. The section between the dotted and solid lines shows the transition of the weighting function. Outside the dotted lines are sections that are not considered in the final h-Creanuis image.

TABLE I
PROBE AND SIGNAL PARAMETERS

Parameter	Value
Transmit frequency	3.5 MHz
Sampling frequency	100 MHz
Active elements number	64
Pitch	264 μm
Kerf	44 μm
Height	5 mm
Transmit focus	70 mm
Elevation focus	23 mm
Apodization	None

dynamic range. Fig. 6 shows the resulting fundamental and second-harmonic h-Creanuis images in comparison with the Creanuis images.

To evaluate the proximity of the two models, the mean deviation is computed as proposed in [2]. It is expressed as

$$\mathrm{MD} = \frac{1}{nm}\sum_{i=1}^{m}\sum_{i=1}^{n}|C(i,j) - hC(i,j)| \quad (4)$$

where n and m are the number of the lines and columns of the C Creanuis and hC h-Creanuis images, respectively. The mean and standard deviation between the Creanuis and h-Creanuis images have been computed for the entire depth of images, but laterally restricted to homogeneous speckle areas. This restriction allows avoidance of the MD evaluation in regions where spikes are present, which would not be fairly taken into account. The measured mean deviations were 2.2% $\pm$ 2.9% and 1.5% $\pm$ 2.5% for the fundamental and second-harmonic images, respectively.

2) Statistical Evaluation: In order to prove that our piecewise PSF convolution and depth apodization approach does not affect the image statistic compared with Creanuis, the statistical distributions of the Creanuis and h-Creanuis images were compared [16], [17]. Creanuis has already been validated in [2]. The resulting distributions are shown in Fig. 7. The root-mean-square error (RMSE) was evaluated between each distribution and the theoretical Rayleigh distribution. It is expressed as

$$\mathrm{RMSE} = \frac{1}{M}\sum_{i=1}^{M}(R_i - X_i)^2 \quad (5)$$

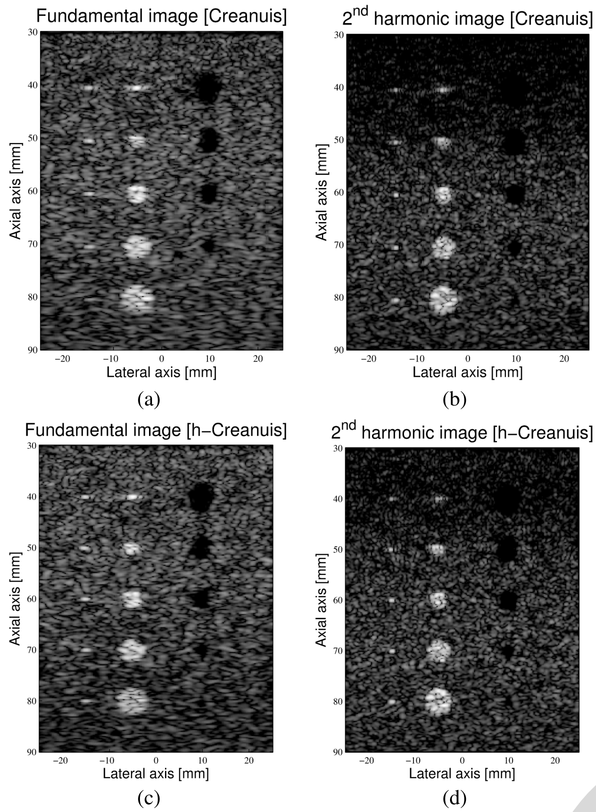

Fig. 6. (a) and (c) Fundamental and (b) and (d) second-harmonic images. The images in (a) and (b) were obtained with Creanuis and those in (c) and (d) with h-Creanuis and six raw images.

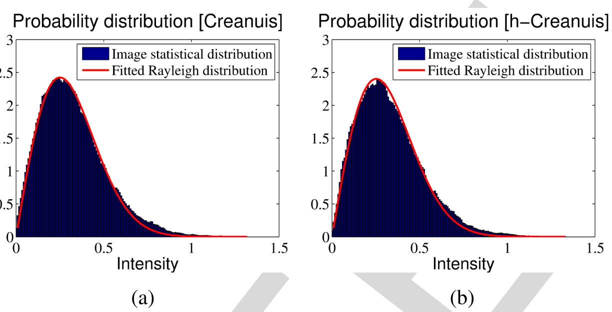

Fig. 7. Obtained statistical distributions for (a) Creanuis and (b) h-Creanuis images.

where M is the number of bins defined in the statistical distribution and R_i (X_i) is the probability of intensity i in the Rayleigh (simulated X image) distribution. The RMSE between these two distributions was also computed. The various values are provided in Table II. We observe that the RMSE between Creanuis and h-Creanuis is low, which means that the statistical behavior of the speckle in the h-Creanuis image has not been changed using the proposed piecewise PSF convolution and depth apodization approach.

3) Optimal Number of PSFs: The cyst phantom was simulated with an increasing number of PSFs to evaluate the optimal number required to obtain an image close to the full acoustic Creanuis image. For each h-Creanuis image, a homogeneous region covering the full depth was extracted and the mean deviation between the Creanuis and h-Creanuis

TABLE II

RMSEs of the Different Simulated Images

Simulated case	RMSE
Creanuis vs. Rayleigh	6.45 %
h-Creanuis vs. Rayleigh	6.82 %
h-Creanuis vs. Creanuis	1.01 %

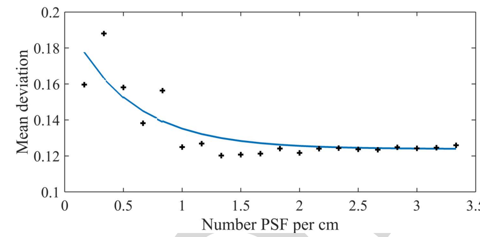

Fig. 8. Evolution of the deviation as a function of the number of PSF per centimeter.

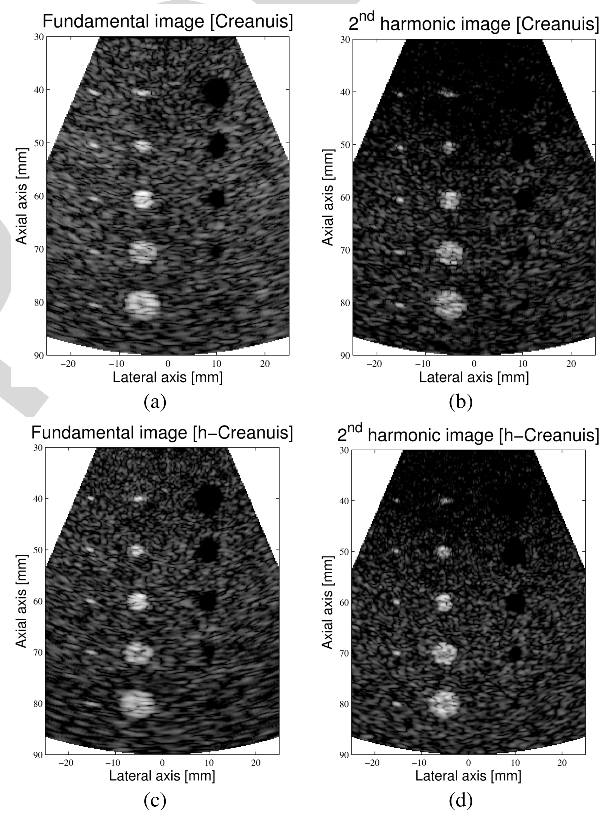

Fig. 9. Simulated fundamental and second-harmonic phased-array images based on six PSFs with (a) and (b) Creanuis and (c) and (d) h-Creanuis.

images was computed. The number of PSFs used was set from 1 to 20. The mean deviation is displayed in Fig. 8 as a function of the number of PSFs per centimeter; when the number of PSFs increases, a smaller section of the medium is covered. Once one PSF per centimeter is obtained, any gain from increasing the number of PSF is insignificant.

4) Phased-Array Imaging: The same cyst medium was imaged using a phased array with a maximum angle of 25°. The resulting h-Creanuis and Creanuis images are presented in Fig. 9. The imaged region is smaller than that using the linear array and the borders of the images are curved. Both the

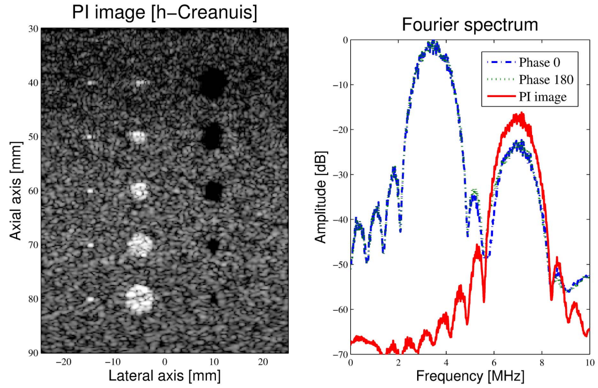

(a) (b)

Fig. 10. (a) PI image and (b) corresponding spectrum based on the six nonlinear raw RF images. The PI image should be compared with the classical second-harmonic image of Fig. 6(d). The +6-dB second-harmonic improvement can be seen in the spectrum.

fundamental and second-harmonic components of the images are very similar, as demonstrated by the mean and standard deviation of $1.7\% \pm 3.3\%$ and $1.5\% \pm 3.6\%$ for fundamental and second-harmonic images, respectively.

5) Nonlinear Imaging With Pulse Inversion: A PI scheme was employed to test the nonlinear simulation used in the proposed methodology. N PSFs are generated for two transmissions: one with a 0° phase and one with a 180° phase. These two resulting h-Creanuis images are summed together to create the PI h-Creanuis image. The obtained image and its spectrum are shown in Fig. 10.

B. 3-D h-Creanuis

A realistic 3-D + t US sequence of a beating heart was simulated with both pyramidal and full phased-array geometry. The medium employed was simulated by applying a realistic strategy based on an experimental 3-D + t heart data set that is available via the Internet [18]. Approximately 1.5 billion scatterers were generated for each 3-D image. In order to clearly observe how the speckle and the simulated sequence evolved, the entire sequence of 34 3-D volumes was normalized before the application of log compression. The dimensions of the Cartesian grid in which the heart was imaged were in the ranges [−90:90] mm, [−90:90] mm, and [0:150] mm, for the x-, y-, and z-directions, respectively. For each 3-D volume, a total of 100 2-D images were simulated using the two strategies. A 45° angle was selected in the lateral and azimuthal directions for the pyramidal and full phased-array geometries.

The 3-D fundamental and 3-D second-harmonic images with a 60-dB dynamic range are displayed in Fig. 11. The improved resolution of the second-harmonic image is visible in these 3-D simulated harmonic images. The beating heart sequence can be directly visualized via the Internet using the proposed desk platform [19].

C. Computation Time

The computation time for the h-Creanuis strategy can be divided into two sections: the first being dependent on the final dimension of the medium used for generating the PSF and the second for simulating the h-Creanuis image. The time required for generating the PSF can be reduced to less than 10 s thanks to the GPU implementation of the nonlinear propagation and the small number of scatterers considered [14].

Implementation of the convolution strategy was performed in MATLAB (The MathWorks, USA). In practice, the convolution is reduced to the section where each weighting function is not null. For the 2-D cyst, the computation time for various quantities of PSFs is shown in Fig. 12. For each quantity of PSFs, 200 simulations were conducted in order to evaluate the mean and standard deviation of the computation time. The total computation time remained under 0.6 s with all the quantities of PSFs tested.

A cluster was used to simulate the 3-D + t sequence. Each 3-D volume was generated separately and less than 1 h was required to obtain the complete sequence of 34 volumes. This computation time can be further decreased using a more efficient implementation in the C++ language.

IV. Discussion

The proposed h-Creanuis model was first evaluated on the cyst phantom. For both linear and phased-array geometries, the mean deviations between the h-Creanuis and Creanuis models are low and reflect the proximity of the two images, even if occasional errors can be observed in the h-Creanuis image, which are highlighted by its standard deviation. The two models were also statistically evaluated and the proximity of the Rayleigh distributions fully validates the h-Creanuis model. This statistical evaluation demonstrates that the speckle statistic has not been changed using our PSF piecewise convolution-based approach. The nonlinear estimation of the image was also evaluated using a PI technique. Once summed, the final PI h-Creanuis image no longer contains a fundamental component but rather exhibits +6 dB in the second-harmonic component, as expected according to the theory [9]. In the simulation of the 3-D+t heart sequence, the motion of the speckle in the whole sequence is coherent in both the fundamental and second-harmonic components.

The h-Creanuis model does suffer from some limitations. The raw images are merged using a weighting function and such functions may cause some discrepancies in the final image. However, we did not observe this effect, even with a limited number of PSFs, most probably because at least three weighted PSF contribute to the signal at each depth. Moreover, the number of PSFs required was evaluated in the cyst phantom. Once one PSF per centimeter was arrived at, the h-Creanuis image could be improved no further. In the Creanuis PSF simulation, as soon as the distance between two scatterers is sufficient, there are no interactions between the scatterers and one simulation of N scatterers is necessary. This simulation is identical to N simulations of one scatterer. Another limitation is that the phased-array geometry was simulated by changing the position of the scatterers. Such an approximation is not valid from an acoustic point of view because the spatial impulse response on the border of the image is no longer correct and the acoustic field is not computed for each angle, which suppresses the impact of

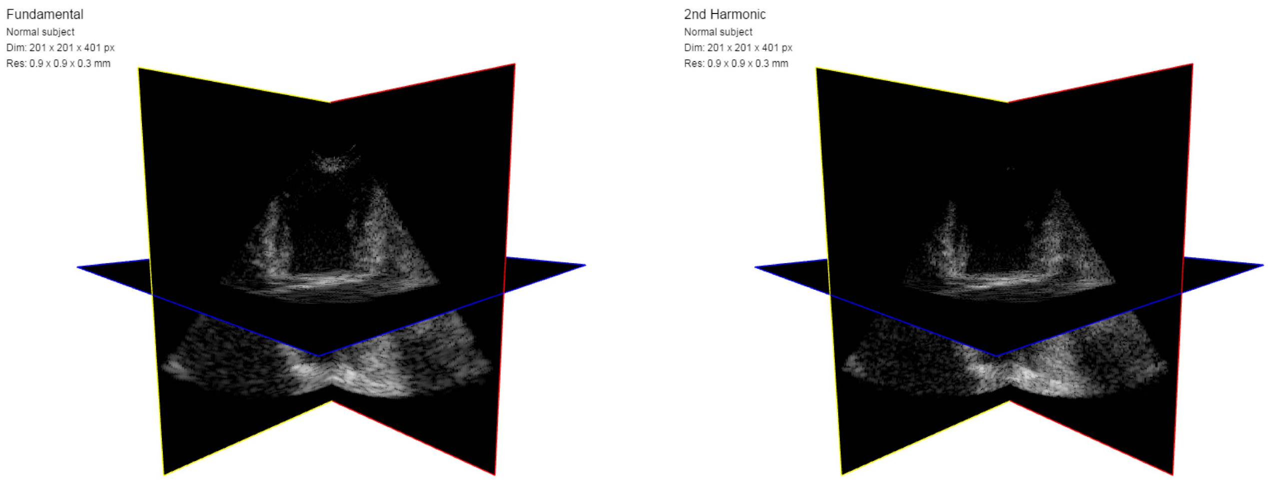

Fig. 11. Obtained fundamental and second-harmonic 3-D images using pyramidal scanning based on the h-Creanuis algorithm. The beating heart can be directly seen online.

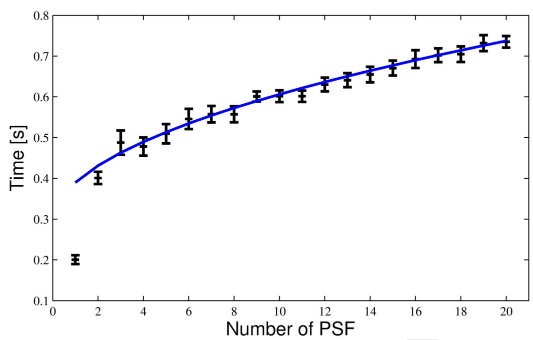

Fig. 12. Computation time as a function of the number of PSFs.

side lobes. Nevertheless, the resulting phased-array images are close to those obtained with Creanuis. The h-Creanuis images have only been compared with Creanuis, which is considered as the reference in this study. The Creanuis software has already been compared with Field II and validated for both deviation and statistical distribution [2]. A number of alternate methods already proposed [3], [12] could be adapted to generate several images with different PSFs and compound them to obtain a PSF varying US image. However, the elementary PSFs used in these studies were not based on physical models and did not consider transducer response, nonlinear propagation, or beamforming.

The most important advantage of the h-Creanuis simulation over the full Creanuis lies in its extremely fast processing capability. For the cyst phantom, 10 s are required for the PSF simulation with Creanuis and less than 0.5 s to generate the final h-Creanuis image, compared with the 30 min required for the full Creanuis acoustic model. Moreover, the second-harmonic image is simulated in the same time, which makes it very promising for future applications, for example, nonlinear imaging schemes and cardiovascular applications.

Future work should aim to integrate the h-Creanuis model into the Creanuis package to allow design of different sequences [20]. The use of h-Creanuis could be twofold: 1) to test a configuration before generating the full acoustic images and 2) to quickly generate a large amount of data. Such a strategy could also be implemented in the virtual imaging platform to decrease the computation time and parallelize the simulation of US image sequences [21]. Moreover, other US applications can be simulated using h-Creanuis as elastography or Doppler imaging.

V. Conclusion

We have proposed a new pseudoacoustic hybrid version of Creanuis (h-Creanuis) to quickly simulate linear or nonlinear RF US images. First, a small number of PSFs are simulated using Creanuis software to obtain PSFs that are related to the nonlinear propagation and the applied beamforming. In the simulation considered in this paper, as soon as one PSF per centimeter is reached, no further gains in the quality of the output image are attained. In future applications, when the transmitted frequency or the image beamforming change, careful attention needs to be paid to the PSF density in h-Creanuis. Second, the convolution of each PSF with the desired medium is realized to obtain the raw nonlinear images. The final h-Creanuis image is created by merging the nonlinear raw RF images using a depth-weighting function. With h-Creanuis, 2-D images can be simulated with linear or phased-array and 3-D images using pyramidal or full phased-array scanning. The 2-D + t and 3-D + t sequences can also be simulated thanks to the low computation time.

Appendix

Mathematical Transformations for Phased-Array and 3-D Geometry

A. Phased-Array Geometry

For phased-array geometry, the position of each scatterer (x, z) needs to be recalculated before generating the nonlinear raw RF images

$$\begin{pmatrix} x \\ z \end{pmatrix}' = R_\theta \begin{pmatrix} x \\ z \end{pmatrix} + \frac{\theta}{\theta_{\max}} x_{\max} \tag{6}$$

where θ is the angle of the scatterer's position in the polar domain, R_θ is the 2-D rotation matrix of angle θ, $\theta_{\max}$ is the maximum angle range of the phased-array scan, and $x_{\max}$ is the maximal lateral dimension of the image.

B. Pyramidal Scanning

Pyramidal scanning is employed to image the 3-D volume using different 2-D phased-array planes. The imaging planes are regularly distributed around the z-axis to image the full volume as illustrated in Fig. 4(a). In practice, it is easier to rotate the scatterers rather than the imaging planes. The 3-D set of scatterers is rotated in the (x, y) direction by an angle φ between each 2-D image simulation

$$\begin{pmatrix}x\\y\end{pmatrix}' = R_\varphi \begin{pmatrix}x\\y\end{pmatrix}^{2}. \tag{7}$$

Equation (6) is then applied to convert the scatterer positions into a 2-D phased-array geometry. The convolution is then conducted to generate one plane of the pyramidal scan. The angle φ is in the range [0°:180°] to regularly map the full 3-D space.

C. Full Phased-Array Scanning

The imaging planes are regularly distributed in an elevated direction (y-axis), as illustrated in Fig. 4(b). For such scanning, the scatterers must first be tilted in the (y, z) plane by an angle ψ for each 2-D image

$$\begin{pmatrix}y\\z\end{pmatrix}' = R_\psi \begin{pmatrix}y\\z\end{pmatrix}. \tag{8}$$

Equation (6) is then applied to convert the scatterer position into a 2-D phased-array geometry. The convolution is then conducted to generate one plane of the pyramidal scan. In this case, angle ψ is in the range $[-\psi_{\max}:\psi_{\max}]$, where $\psi_{\max}$ is the maximal range on the phased-array geometry in the (y, z) direction.

References

[1] J. A. Jensen and N. B. Svendsen, "Calculation of pressure fields from arbitrarily shaped, apodized, and excited ultrasound transducers," *IEEE Trans. Ultrason., Ferroelectr., Freq. Control*, vol. 39, no. 2, pp. 262–267, Mar. 1992.

[2] F. Varray, O. Basset, P. Tortoli, and C. Cachard, "CREANUIS: A nonlinear radiofrequency ultrasound image simulator," *Ultrasound Med. Biol.*, vol. 39, no. 10, pp. 1915–1924, 2013.

[3] A. Marion and D. Vray, "Toward a real-time simulation of ultrasound image sequences based on a 3-D set of moving scatterers," *IEEE Trans. Ultrason., Ferroelectr., Freq. Control*, vol. 56, no. 10, pp. 2167–2179, Oct. 2009.

[4] H. Gao *et al.*, "A fast convolution-based methodology to simulate 2-D/3-D cardiac ultrasound images," *IEEE Trans. Ultrason., Ferroelectr., Freq. Control*, vol. 56, no. 2, pp. 404–409, Feb. 2009.

[5] H. Gao, T. Hergum, H. Torp, and J. D'hooge, "Comparison of the performance of different tools for fast simulation of ultrasound data," *Ultrasonics*, vol. 52, no. 5, pp. 573–577, 2012.

[6] G. F. Pinton, J. Dahl, S. Rosenzweig, and G. E. Trahey, "A heterogeneous nonlinear attenuating full-wave model of ultrasound," *IEEE Trans. Ultrason., Ferroelectr., Freq. Control*, vol. 56, no. 3, pp. 474–488, Mar. 2009.

[7] B. E. Treeby, M. Tumen, and B. T. Cox, "Time domain simulation of harmonic ultrasound images and beam patterns in 3D using the k-space pseudospectral method," in *Medical Image Computing and Computer-Assisted Intervention*, vol. 6891. 2011, pp. 363–370. AQ:5

[8] F. Varray, A. Ramalli, C. Cachard, P. Tortoli, and O. Basset, "Fundamental and second-harmonic ultrasound field computation of inhomogeneous nonlinear medium with a generalized angular spectrum method," *IEEE Trans. Ultrason., Ferroelectr., Freq. Control*, vol. 58, no. 7, pp. 1366–1376, Jul. 2011.

[9] D. H. Simpson, C. T. Chin, and P. N. Burns, "Pulse inversion Doppler: A new method for detecting nonlinear echoes from microbubble contrast agents," *IEEE Trans. Ultrason., Ferroelectr., Freq. Control*, vol. 46, no. 2, pp. 372–382, Mar. 1999.

[10] R. J. Eckersley, C. T. Chin, and P. N. Burns, "Optimising phase and amplitude modulation schemes for imaging microbubble contrast agents at low acoustic power," *Ultrasound Med. Biol.*, vol. 31, no. 2, pp. 213–219, 2005.

[11] R. Shams, R. Hartley, and N. Navab, "Real-time simulation of medical ultrasound from CT images," in *Medical Image Computing and Computer-Assisted Intervention* (Lecture Notes in Computer Science), vol. 5242, D. Metaxas, L. Axel, G. Fichtinger, and G. Székely, Eds. Berlin, Germany: Springer, 2008, pp. 734–741. AQ:6

[12] O. Kutter, R. Shams, and N. Navab, "Visualization and GPU-accelerated simulation of medical ultrasound from CT images," *Comput. Methods Programs Biomed.*, vol. 94, no. 3, pp. 250–266, 2009.

[13] F. Varray, H. Liebgott, C. Cachard, and D. Vray, "Fast simulation of realistic pseudo-acoustic nonlinear radio-frequency ultrasound images," in *Proc. IEEE Ultrason. Symp.*, Sep. 2014, pp. 2217–2220.

[14] F. Varray, C. Cachard, A. Ramalli, P. Tortoli, and O. Basset, "Simulation of ultrasound nonlinear propagation on GPU using a generalized angular spectrum method," *EURASIP J. Image Video Process.*, vol. 17, no. 1, 2011. AQ:7

[15] J. A. Jensen and P. Munk, "Computer phantoms for simulating ultrasound B-mode and CFM images," in *Proc. 23rd Acoust. Imag. Symp.*, 1997, pp. 75–80.

[16] T. D. Mast, "Convolutional modeling of diffraction effects in pulse-echo ultrasound imaging," *J. Acoust. Soc. Amer.*, vol. 128, no. 3, pp. EL99–EL104, 2010.

[17] R. F. Wagner, S. W. Smith, J. M. Sandrik, and H. Lopez, "Statistics of speckle in ultrasound B-scans," *IEEE Trans. Sonics Ultrason.*, vol. 30, no. 3, pp. 156–163, May 1983.

[18] M. Alessandrini *et al.*, "A pipeline for the generation of realistic 3D synthetic echocardiographic sequences: Methodology and open-access database," *IEEE Trans. Med. Imag.*, vol. 34, no. 7, pp. 1436–1451, Jul. 2015.

[19] F. Varray. (2015). *Simulated Beating Heart Volume Using, h-Creanuis*. [Online]. Available: http://desk.creatis.insa-lyon.fr/hcreanuis/ AQ:8

[20] F. Varray. (2013). *Creanuis Webpage*. [Online]. Available: https://www.creatis.insa-lyon.fr/site/en/CREANUIS

[21] T. Glatard *et al.*, "A virtual imaging platform for multi-modality medical image simulation," *IEEE Trans. Med. Imag.*, vol. 32, no. 1, pp. 110–118, Jan. 2013.

François Varray was born in Montpellier, France, in 1985. He received the Engineering Diploma from the Ecole des Mines de Saint-Etienne, Saint-Étienne, France, in 2008, the master's degree in image and signal processing, and the Ph.D. degree with a focus on nonlinear ultrasound simulation in 2011. AQ:9

His Ph.D. research was realized in co-agreement between the Centre de Recherche en Acquisition et Traitement de l'Image pour la Santé (CREATIS), Lyon, France and the MSD Laboratory, Florence, Italy. Since 2013, he has been an Associate Professor with CREATIS. His research interests include the nonlinear ultrasound propagation simulation, nonlinear image simulation, multi-resolution motion estimation, cardiac imaging, and photoacoustic imaging. AQ:10

Olivier Bernard received the M.Sc. degree in electrical engineering and the Ph.D. degree in medical image processing from the Université de Lyon, Lyon, France, in 2006.

He was a Postdoctoral Research Fellow with the Federal Polytechnic Institute of Lausanne, Lausanne, Switzerland, headed by Prof. M. Unser in 2007. In 2007, he became an Associate Professor with the Université de Lyon and a member of the Centre de Recherche en Acquisition et Traitement de l'Image pour la Santé, Université de Lyon. In 2013, he was an Invited Professor with the Federal Polytechnic Institute of Lausanne headed by Prof. J. P. Thiran. His current research interests include medical image processing with a particular attention to cardiac modalities, image segmentation, motion analysis, statistical modeling, sampling theories, and machine learning.

Dr. Bernard received the special mention (second prize) for the best Ph.D. in France by the IEEE Engineering in Medicine and Biology Society in 2008. He is an Associate Editor of the IEEE TRANSACTIONS ON IMAGE PROCESSING and was a member of the Technical Committee of the IEEE International Conference on Image Processing and the IEEE International Symposium on Biomedical Imaging.

Sonia Assou was born in Lyon, France, in 1992. She received the Engineering Diploma with a specialization in applied mathematics from Polytech Lyon, Villeurbanne, France, in 2016. She is about to prepare a Ph.D. thesis at Renault in which the main topics are automatic machine learning, big data, and model reduction for computational fluid dynamic problems.

Christian Cachard received the Ph.D. degree in acoustics from the Institut National des Sciences Appliquées de Lyon, Lyon, France, in 1988, with a minor in signal processing for underwater acoustics.

He is currently a Professor with the Electrical Engineering Department, Technical Institute, Université Claude Bernard Lyon 1, Lyon. Since he joined the Centre de Recherche en Acquisition et Traitement de l'Image pour la Santé, his domain of interest includes ultrasound medical imaging, ultrasound contrast agent imaging, ultrasound radio frequency processing, microtools localization in 3-D ultrasound data, and 2-D matrix arrays for 3-D imaging. He has co-authored 38 papers in peer-reviewed journals and has supervised 18 Ph.D. students.

Didier Vray is currently a Professor of Signal Processing and Computer Sciences with the Institut National des Sciences Appliquées de Lyon, Lyon, France. His main research interest focuses on ultrasound medical imaging, since he joined the Centre de Recherche en Acquisition et Traitement de l'Image pour la Santé, Université de Lyon, Lyon. He has authored over 100 scientific publications and two issued patents in this field. His current research interests include vascular imaging, flow imaging, tissue motion estimation, and bimodality ultrasound/optics imaging.

AUTHOR QUERIES

AUTHOR PLEASE ANSWER ALL QUERIES

PLEASE NOTE: We cannot accept new source files as corrections for your paper. If possible, please annotate the PDF proof we have sent you with your corrections and upload it via the Author Gateway. Alternatively, you may send us your corrections in list format. You may also upload revised graphics via the Author Gateway.

AQ:1 = Please confirm/give details of funding source.
AQ:2 = Please confirm whether the corresponding author information is correct as set.
AQ:3 = Please confirm whether the edits made in the current affiliation of all the authors are OK as set.
AQ:4 = Please confirm “and has theoretically to be updated in” is changed as “and has to theoretically be updated in” as per editing aspect.
AQ:5 = Please confirm the volume no. for ref. [7]. Also provide the publisher name and publisher location.
AQ:6 = Please confirm the volume no. for ref. [11].
AQ:7 = Please provide the page range for ref. [14].
AQ:8 = Please confirm the title for refs. [19] and [20].
AQ:9 = Please specify the University name for the master’s and Ph.D. degrees of the author “Francois Varray.”
AQ:10 = Please confirm whether the edits made in the sentence "His research interests include . . . photoacoustic imaging.” has been deleted, as it does not seem to be a part of the author biography. Please check.
AQ:11 = Please confirm “pour la Santé.” is changed as “pour la Santé, Université de Lyon.” as per editing aspect.
AQ:12 = Please provide the location for Renault.
AQ:13 = Please confirm whether the edits made in the sentence “Didier Vray . . . pour la Santé” are OK.
AQ:14 = Please confirm “pour la Santé.” is changed as “pour la Santé, Université de Lyon, Lyon.” as per editing aspect.